Article

Chinese Science Bulletin

Geophysics

February 2012 Vol.57 No.5: 500–510
doi: 10.1007/s11434-011-4851-y

Analysis of ionospheric anomalies before the 2011 M_w 9.0 Japan earthquake

YAO YiBin*, CHEN Peng, WU Han, ZHANG Shun & PENG WenFei

School of Geodesy and Geomatics, Wuhan University, Wuhan 430079, China

Received July 25, 2011; accepted October 8, 2011; published online November 19, 2011

On March 11, 2011, a large earthquake of M_w=9.0 occurred near the east coast of Honshu, Japan. This paper investigates pre-earthquake ionospheric anomalies during the earthquake period, using data from global navigation satellite systems and ionosonde stations near the epicenter. A clear anomaly that occurred on March 8 lasted 6 hours. Eliminating ionospheric anomalies that may have been caused by solar activities and magnetic storms, we believe that a positive anomaly on March 8 was very possibly an ionospheric precursor. The affected ionospheric area on March 8, which is evident on a vertical total electron content distribution map, extended to 50° in longitude and 20° in latitude, with length ratio approximately 3∶1. The anomaly peak arose from 15:00–19:00 LT, and its location did not coincide with the vertical projection of the epicenter, but was instead to its south. Corresponding ionospheric anomalies are also observed in the magnetically conjugated region. There were no obvious ionospheric anomalies in other parts of the world. To analyze changes in the ionospheric anomaly, computerized ionospheric tomography technology was used to invert the spatial and temporal distribution of electron density in the ionosphere. The ionospheric anomaly on March 8, 2011 is suggested to be an ionospheric precursor of the March 11 earthquake in Japan.

earthquake, vertical total electron content, ionospheric anomaly, ionospheric tomography, global positioning system

Citation: Yao Y B, Chen P, Wu H, et al. Analysis of ionospheric anomalies before the 2011 M_w 9.0 Japan earthquake. Chin Sci Bull, 2012, 57: 500–510, doi: 10.1007/s11434-011-4851-y

Earthquakes are one of the most destructive and harmful natural disasters, and can cause tremendous loss of human life. Seismologists are committed to earthquake monitoring and prediction, and there have been some successful cases of earthquake prediction. Such prediction, however, especially in the short term, is still in the exploratory stage [1]. To predict earthquakes accurately, many scholars have been exploring new earthquake monitoring and prediction methods. Seismo-ionospheric anomalies before large earthquakes have been intensively studied [2–6]. These anomalies have a relatively stable time scale, which makes them feasible for short-term prediction. Dramatic ionospheric changes may be caused by many factors, such as solar activity and geomagnetic field changes. Therefore, the core technical problem for earthquake prediction is to distinguish ionospheric disturbances associated with earthquakes from those caused by other factors [7–12].

Leonard and Barnes [6] discovered ionospheric disturbances before the 1964 earthquake in Alaska, USA, which attracted attention to the relationship between pre-earthquake ionospheric anomalies and earthquakes for the first time, and provided a new method of earthquake prediction. Weaver et al. [13] found ionospheric disturbances during the 1969 Kurile Islands earthquake. Antsilevich [14] found that ionospheric electron density increased during the 1966 Tashkent earthquake. Pulinets [15–17] discerned disturbances in several ionospheric parameters preceding strong shocks between 1979 and 1981. After investigating ionospheric changes associated with 50 M 5.0+ earthquakes, he confirmed that the f_oF_2 declined significantly before the earthquakes; the ionospheric anomaly area corresponded to the hypocentral region, but the most affected area in the ionosphere did not coincide with the vertical projection of the epicenter of the proceeding earthquake. Liu et al. [18]

*Corresponding author (email: ybyao@whu.edu.cn)

examined variations in f_oF_2 before $M \geqslant 6.0$ earthquakes from 1994–1999 in Taiwan. The result showed that precursors, in the form of recorded f_oF_2 falling below its associated lower bound around 12:00–17:00 LT, appeared 1–6 days prior to those earthquakes. Based on data from the geomagnetic network and ionospheric observatories in China, Ding et al. [19] compared the anomaly distribution, characteristics of geomagnetic variation field, and ionospheric f_oF_2 before the Mani M_S 7.5 earthquake on Nov. 8, 1997, and the Kunlunshan M_S 8.1 earthquake on Nov. 14, 2001. Their results showed that the temporal and spatial characteristics of short term and imminent anomalies of the geomagnetic field and ionosphere are consistent. Le et al. [20] did a statistical study of pre-earthquake ionospheric anomalies for 736 $M \geqslant$ 6.0 earthquakes across the globe, from 2002–2010. Based on hundreds of seismic cases using ground-based and satellite measurements, Pulinets et al. [7] summarized the major characteristics of observed ionospheric anomalies.

Most researchers have used the ionosonde f_oF_2 to analyze pre-earthquake ionospheric anomalies, but an ionosonde can only detect the distribution of ionospheric electron density over points, which does not fully reflect wide-ranging changes in the ionosphere [15]. Global navigation satellite systems (GNSS) represent a new technology that obtains accurate total electron content (TEC) values from satellite to receiver, and continuously monitors ionospheric changes over a wide geographic range. Calais et al. [21] were the first to use GNSS to detect ionospheric anomalies before earthquakes. Using GPS data recorded by the permanent GNSS network in southern California, they analyzed TEC disturbances during the several days preceding and following the M_W = 6.7 Northridge earthquake on January 17, 1994. Zaslavski et al. [22] tested the correlation between seismic activity and ionospheric disturbances by statistically studying TEC from TOPEX–POSEIDON satellites. Liu et al. [18] examined pre-earthquake ionospheric anomalies using TEC, during all 20 $M \geqslant 6.0$ earthquakes in the Taiwan area, from September 1999 to December 2002. Wu et al. [23] statistically analyzed TEC variations before three strong earthquakes in Asia, and found anomalous TEC disturbances over a seismic preparation zone in the 10 days before these earthquakes. Several researchers [24–30] analyzed ionospheric vertical total electron content (VTEC) anomalies before the May 12, 2008 Wenchuan earthquake, using different methods.

To aid understanding of the full range of temporal and spatial distributions of ionospheric electron density, GNSS-based computerized ionospheric tomography (CIT) technology has gradually developed over the past decade [31–36]. Using the new CIT technology, we can reconstruct the 3-dimensional (3-D) spatial structure of the ionosphere. Using GPS data from Chinese GNSS stations and CIT, Wen et al. [37] studied temporal and spatial changes in ionospheric electron density over the China region on August 18 and August 21, 2003, when magnetic storms occurred. Thampi et al. [38] used CIT to investigate the summer night ionospheric anomaly in mid-latitudes.

At 14:46 LT, March 11, 2011, a large earthquake M_W=9.0 occurred near the east coast of Honshu, Japan (38.1°N, 142.6°E), at 20 km depth. This earthquake may be the strongest ever recorded in Japan.

This paper investigates pre-earthquake ionospheric anomalies and their temporal and spatial characteristics during the March 11 earthquake, using data from GNSS and ionosonde stations near the epicenter. After eliminating ionospheric anomalies that may have been caused by solar activities or magnetic storms, and considering the spatial distribution of the anomalous area, we believe that a positive anomaly on March 8, 2011 is the most likely ionospheric precursor. CIT is used to show the 3-D ionospheric electron density distribution and its changes near the epicenter. The result is consistent with that derived from VTEC and f_oF_2 data. This provides further confirmation that an anomaly on March 8, 2011 was a possible ionospheric precursor. This finding aids the understanding of earthquake monitoring and forecasting based on the ionosphere.

1 GNSS-based ionospheric data processing methods

In this paper, GNSS-based ionospheric research methods are executed through self-compiled software, and used to analyze ionospheric electron density during the earthquake period. Following is a brief introduction to the data processing methods.

Because the ionospheric delay of the GNSS signal is inversely proportional to the square of signal frequency, the TEC along the signal propagation path can be calculated from GNSS dual frequency observations [39]. There are three ways to calculate ionospheric TEC: pseudorange, carrier phase and carrier-smoothed code pseudorange. Pseudorange has considerable noise, and is susceptible to multipath effects. Carrier phase introduces too much ambiguity parameters, which may cause difficulty in the calculation of TEC. Therefore, the most widely used method of calculating TEC is the carrier-smoothed code pseudorange. The TEC calculation can be written as

$$\mathrm{TEC} = \frac{f_1^2 f_2^2}{40.28\left(f_1^2 - f_2^2\right)}\left(\tilde{P}_2 - \tilde{P}_1 + \Delta b_k + \Delta b^s\right), \tag{1}$$

where $\tilde{P}_1$, $\tilde{P}_2$ are carrier-smoothed code pseudorange measurements on L1 and L2 frequencies, respectively; Δb_k is the difference of receiver hardware delays between the two frequencies; and Δb^s is the difference in satellite hardware delays between the two frequencies. We project the TEC of the signal propagation direction to the zenith direction at the puncture point, then establish a regional ionospheric model and solve the model parameters at 2-h intervals. Hardware delays of the system are solved as model parameters.

When using the method described above to calculate TEC, it is assumed that all ionospheric electrons are concentrated in an infinitely thin layer at a certain altitude (typically 350 km), which only provides overall changes in ionospheric electron content. To understand the ionosphere more fully, the distribution of the ionospheric electron density at different altitudes is necessary. GNSS-based CIT, a new method for advancing this understanding, can reconstruct the 3-D or even 4-D structure of the ionosphere.

According to its definition, TEC is the line integral of electron density along the signal propagation path and can be written as

$$\mathrm{TEC} = \int_l Ne(\vec{r},t)\mathrm{d}s, \tag{2}$$

where *Ne* is the electron density along the signal propagation path *l*. GNSS-based ionospheric CIT uses a series of TECs along *l* (according to eq. (1)) to inverse the temporal and spatial distribution of ionospheric electron density.

From eq. (2), the relationship between TEC and *Ne* is nonlinear, thus the first step of the inversion process is to discretize eq. (2). After discretization, we get the following:

$$\vec{y} = A \cdot \vec{x} + \vec{\varepsilon}. \tag{3}$$

The physical meaning of each parameter in eq. (3) is determined by the selected base function. General forms of base functions are divided into local base and global base functions. We use a local base function, i.e. a pixel-based ionospheric CIT method, to calculate electron density. The electron density of each pixel within the inversion region is considered a constant. Therefore, in eq. (3), A is the coefficient matrix constituted by intercepts when GNSS signals pass through the pixels of the ionosphere; $\vec{y}$ is the observation vector constituted by the TEC along each GNSS signal propagation path; $\vec{x}$ is the parameter vector constituted by the electron density of each pixel; $\vec{\varepsilon}$ is the noise vector of observations.

Using the above equation for ionospheric CIT, the coefficient matrix A is a huge sparse matrix and is usually rank deficient. Therefore, the equation cannot be solved by the common method of Kaley inverse. The most common approach is to use an empirical model, such as the international reference ionosphere model, as the initial value of iteration, to obtain the electron density of the inversion region. The iteration result depends on the accuracy of TECs that pass through the ionospheric region and the accuracy of the initial value. When an ionospheric anomaly occurs, the initial value from the empirical model will greatly deviate from the true value, and the inversion accuracy will be reduced. According to the current state of ionospheric CIT, a new solution is introduced to overcome these two problems. First, constraint equations and virtual observatories are used to overcome the problem of rank deficiency. Then, we decompose eq. (3) and constraint equations by singular value decomposition. Then we use the Tikhonov regularization to approximate the electron density. The regularization parameter for Tikhonov regularization is determined by the generalized cross validation criterion. We use a related model for anomaly detection and repair of the electron density approximation. Finally, the repaired approximation is used as the initial value of the selected iterative reconstruction method, to calculate the final electron density [31,40,41].

Given the non-negativity of electron density, we inverse it by the multiplicative algebraic reconstruction technique. The iterative formula can be written as

$$x_j^{(k+1)} = x_j^{(k)} \left(\frac{y_i}{\left\langle a_i, x^{(k)} \right\rangle} \right)^{\frac{\gamma_0 \cdot a_{ij}}{A}}, \tag{4}$$

where $x^{(k)}$ is the unknown parameter of the kth iteration; a_i is the ith row of A; γ_0 is the relaxation factor of each iteration, with $0 < \gamma_0 < 1$.

2 Analysis and discussion

To investigate pre-earthquake ionospheric anomalies during the March 11 earthquake, we used dual-frequency observations from 20 GNSS stations near the epicenter to calculate the VTEC time series in the region. The time interval of the GNSS observations was 15 min. To illustrate abnormal ionospheric changes, we took VTEC data from four GNSS stations (MIZU, TSKB, USUD, and AIRA) and f_oF_2 data from one ionosonde station (Okinawa/Ogimi) to exemplify the pre-earthquake anomalies. Figure 1 shows the locations of the Okinawa/Ogimi ionosonde, the GNSS stations, and the epicenter of the March 11 earthquake. To analyze the anomalies, we detected outliers in the VTEC time series of the GNSS stations and the f_oF_2 ionosonde time series, and

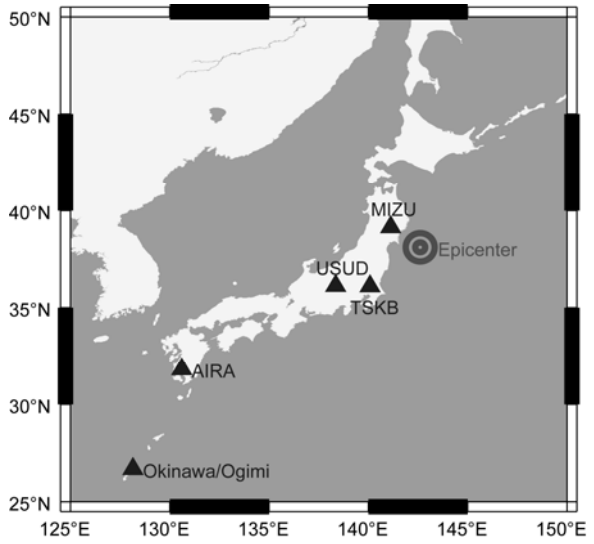

Figure 1 Locations of the Okinawa/Ogimi ionosonde, four GNSS stations, and the epicenter of the March 11, 2011 Japan earthquake.

also used CIT to reconstruct the temporal and spatial distribution of ionospheric electron density. Solar and magnetic activity was also considered when ionospheric anomalies occurred.

2.1 VTEC and f_oF_2 time series analysis

If there is no great change in the space environment, day-to-day variability of the ionosphere is generally stable, and it does not change much over a short time. Under the assumption of a normal distribution with mean μ and standard deviation σ for the VTEC and f_oF_2, we applied the sliding window-based method to calculate the median and standard deviation, using VTEC or f_oF_2 data a few days before and after the current day. Taking 2σ as the tolerance, an observed VTEC or f_oF_2 value outside the associated upper or lower bound is regarded as an ionospheric anomaly at the observation time [42–45].

Figure 2 shows the VTEC time series over the MIZU station, from February 26 to March 10 (1–13 days prior to the earthquake). MIZU is the closest station to the epicenter. The original data from March 11 to March 15 were missing because of the earthquake. Figure 2 shows that there were some positive anomalies during March 2–3 and significant positive anomalies on March 8 (3 days before the earthquake).

Figures 3 and 4 show an 18-day VTEC time series over the USUD and TSKB stations, respectively, which encompasses the earthquake event. The data are similar to the MIZU station. There were some positive anomalies during March 2–3 and significant positive anomalies on March 8. The VTEC time series clearly increased on the day of the earthquake and for 2 days afterward, then returned to normal on March 15.

Figure 5 shows the analogous 18-day VTEC time series over the AIRA station. Compared with the other three GNSS

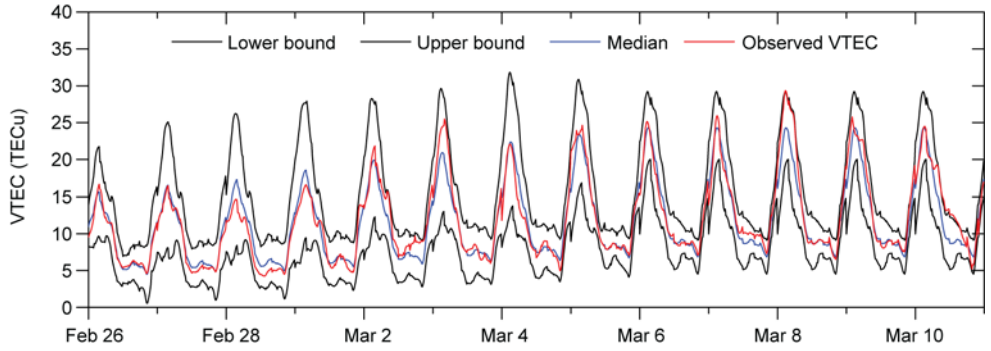

Figure 2 VTEC time series over MIZU station, from February 26 to March 10.

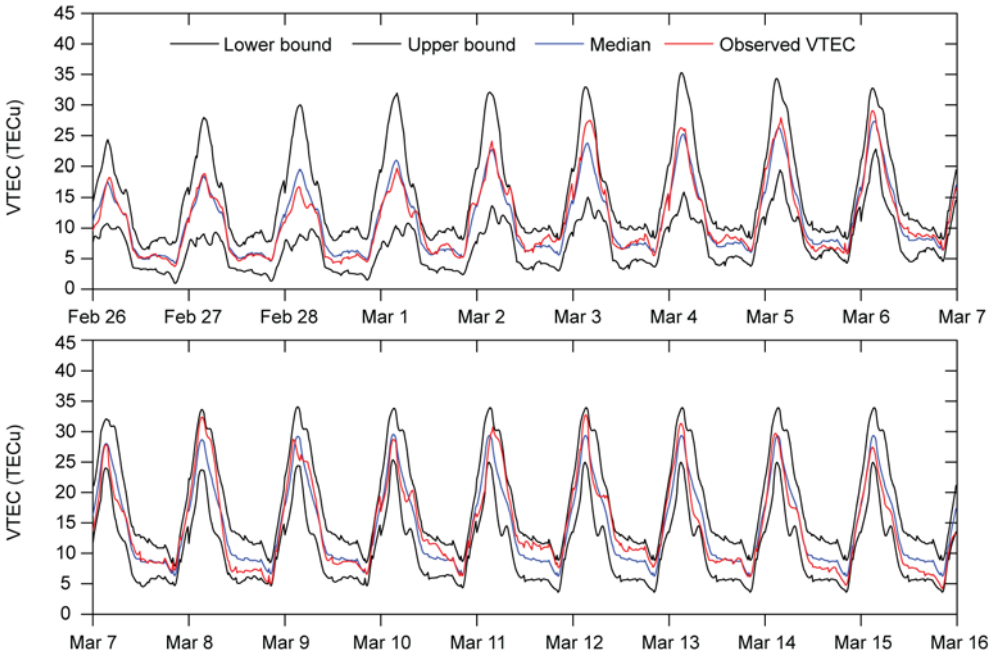

Figure 3 VTEC time series over the USUD station, from February 26 to March 15.

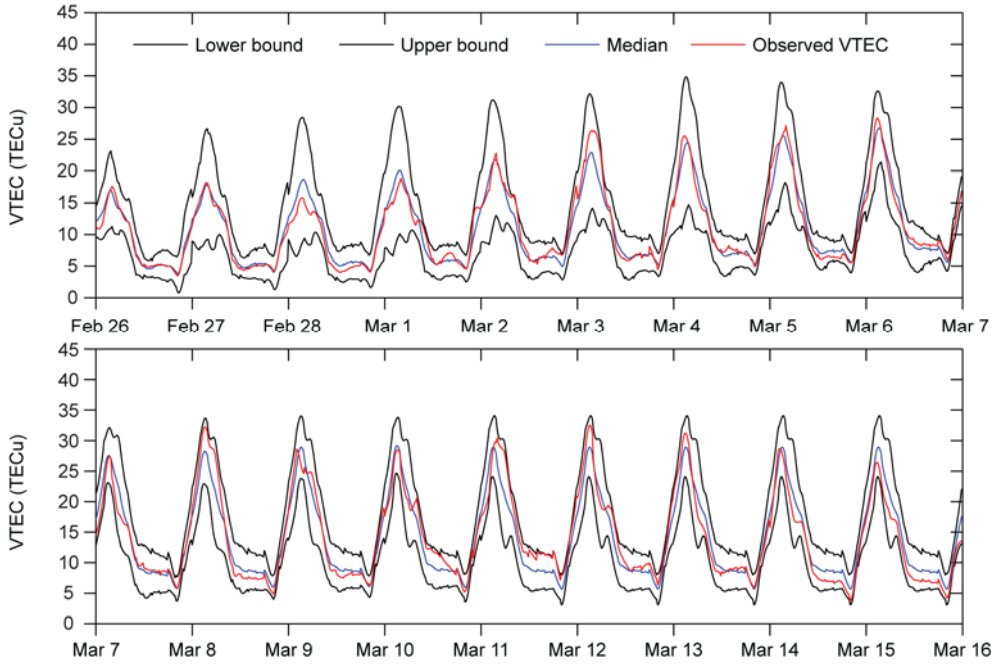

Figure 4 VTEC time series over the TSKB station, from February 26 to March 15.

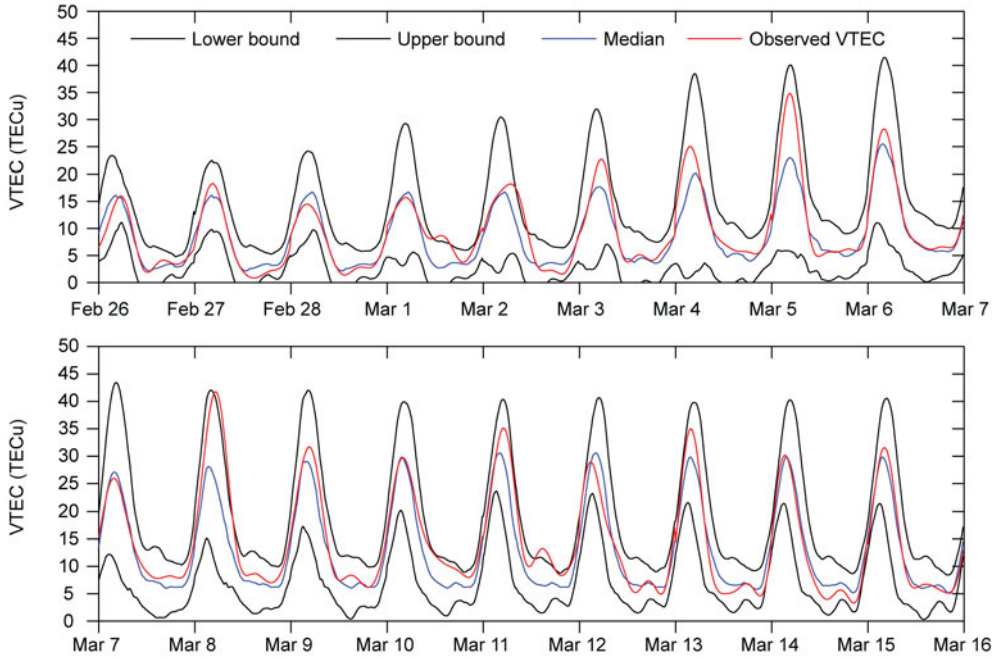

Figure 5 VTEC time series over the AIRA station, from February 26 to March 15.

stations, the AIRA station is further from the epicenter, but closer to the equator. Previous studies have found that the most affected area in the ionosphere does not coincide with the vertical projection of the epicenter of the proceeding earthquake. This area is, however, generally located on the equator side of the epicenter. The VTEC time series at the AIRA station is consistent with previous studies. From Figure 5, the VTEC anomalies at the AIRA station were more significant than at the other three stations, and the VTEC on March 5 exceeded those a few days before and after.

To verify the reliability of the above VTEC analysis, Figure 6 shows the 18-day f_oF_2 time series from the Japan Okinawa/Ogimi ionosonde station during the period around the earthquake. The time is JST (Japan Standard Time). The coordinate of the Okinawa/Ogimi station is 26.68°N, 128.15°E, which is 10° south of the epicenter. Figure 6 shows that there

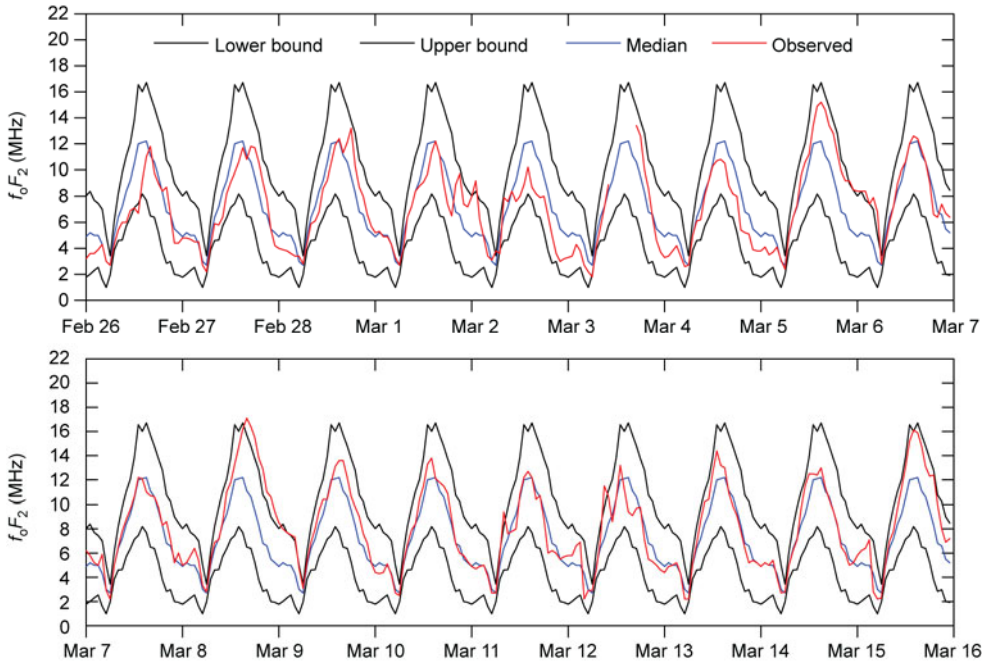

Figure 6 f_oF_2 time series over the Okinawa/Ogimi ionosonde station, from February 26 to March 15.

were positive anomalies during March 1–2. The f_oF_2 on March 8 were visibly larger than the other days, and anomalies persisted for more than 10 hours. The f_oF_2 data are consistent with the VTEC analysis above.

Because solar and geomagnetic activities strongly affect the ionosphere, the solar terrestrial environment should be taken into account when identifying the source of ionospheric anomalies [46]. Figure 7 shows time series of solar wind speed (V_{sw}), interplanetary magnetic field (IMF) B_z component in GSM coordinates, $F_{10.7}$ index, *Dst* index, and *Kp* index, from February 26 to March 15. A rapid increase of V_{sw} occurred on March 1, reaching 700 km/s on March 2. Then, V_{sw} began a slow daily decrease, and was less than 400 km/s after March 8. From the day of the earthquake, it gradually increased, maintaining 500–600 km/s, and then gradually decreased on March 15. The IMF B_z component showed very large variations over a short time on March 1, and relatively small fluctuations a few days before and after the earthquake. The variations on the remaining days were within ±5 nT. $F_{10.7}$ indexes were above 100 during March 1–15 and reached 155 on March 8, indicating strong solar radiation. There were geomagnetic disturbances on March 1–2 and March 10–12 ($Kp>4$; $Dst<-40$ nT). The geomagnetic field on the other days was low ($Kp\leqslant 3$; $Dst\geqslant -20$).

We analyzed the causes of the ionospheric anomalies before the earthquake, and attempted to exclude anomalies that may have been caused by solar or magnetic field activities. During March 1–2, the *Dst* index reached −60 nT, and the *Kp* index exceeded 5, indicating the likelihood of a geomagnetic storm on these 2 days. The V_{sw} surged from 300 km/s to 700 km/s on March 1, and the IMF B_z component also varied markedly, indicating intense solar activity on this day. Therefore, we believe that the ionospheric anomalies on these 2 days were caused by solar activity and a magnetic storm. On March 8, the VTEC time series from the four GNSS stations and the f_oF_2 time series from the ionosonde both showed significant and persistent positive anomalies. Figure 7 shows that on March 8, *Kp* did not exceed 2 and *Dst* was greater than −20 nT, thus the geomagnetic field was very quiet. The V_{sw} was less than 400 km/s, indicating a weak solar wind. However, the $F_{10.7}$ index on March 8 reached 155, signifying the strongest solar radiation of the period. There was a certain relationship between the ionospheric anomalies and the intense solar activity. Therefore, further analysis is needed to determine whether the ionospheric anomalies on March 8 were caused by the earthquake. There were also ionospheric anomalies during March 11–13. Nevertheless, solar and geomagnetic field activities were intense during these days, and we consider these anomalies to be caused by solar and geomagnetic field activities.

2.2 Global distribution of abnormal VTEC on March 8

The global spatial distribution of ionospheric anomalies on March 8 is presented for additional investigation of the causes of those anomalies on March 8. In particular, the GNSS TEC of the global ionosphere map was used to find the anomalies. We calculated the moving VTEC median and standard deviation of 1–10 previous days as a background value. If the difference between the observed VTEC and its median value, designated as ΔVTEC, was less than

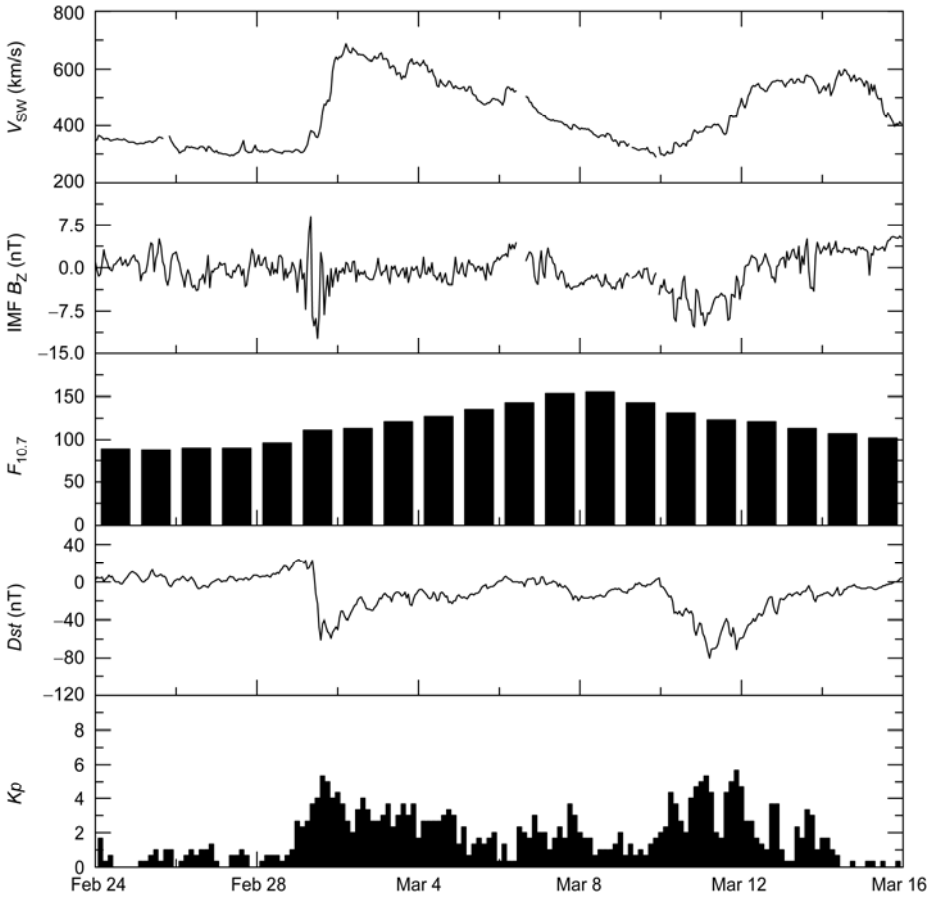

Figure 7 Time series (from top to bottom) of solar wind speed (V_{sw}), interplanetary magnetic field (IMF) B_z component in GSM coordinates, $F_{10.7}$ index, *Dst* index, and *Kp* index, from February 26 to March 15.

twice the standard deviation, we set ΔVTEC=0. ΔVTEC>0 indicates positive anomalies; ΔVTEC<0 indicates negative anomalies.

Figure 8 shows global ΔVTEC maps from 04:00–14:00 UT on March 8, with a time interval of 2 h. A red star represents the epicenter. We can clearly see changes in ionospheric anomalies, which began to appear at 04:00 UT. The most affected area was located roughly 170°E, 25°N, with maximum ΔVTEC of 8.9 TECu. This area expanded and moved slowly west. At 06:00 UT, the area of maximum effect was at 140°E, 30°N, with maximum ΔVTEC of 14.8 TECu. Corresponding ionospheric effects were observed in the magnetically conjugated region. At 08:00 UT, the anomaly reached maximum extent and magnitude. The effect expanded in area, from 90°E–180° and 12.5°–37.5°N. The ratio between the length and width of this area was roughly 3∶1. The location of maximum effect was at 130°E, 30°N, with maximum ΔVTEC of 17.3 TECu. The extent and magnitude of anomalies in the conjugated region also significantly increased. At 10:00 UT, anomalies began to weaken, with maximum ΔVTEC of 13.6 TECu. At 12:00 UT, the weakening continued and, after 14:00 UT, the anomalies gradually disappeared. The area of maximum effect in the ionosphere was near the epicenter, on its equatorward side. The duration of the ionospheric anomalies was more than 8 h. There was no significant ionospheric VTEC anomaly in the rest of the world at this time. Ionospheric anomalies caused by solar or magnetic field activities generally manifest over a wider geographic range. The ionospheric anomalies observed on March 8, however, appeared only near the epicenter, and their duration was comparatively long. This provides further evidence that the ionospheric anomalies on March 8 were associated with the proceeding earthquake.

2.3 Using CIT technology to reconstruct the temporal and spatial distribution of ionospheric electron density during March 7–9

To understand changes in ionospheric electron density at different altitudes on March 8, we reconstructed electron density distribution images at 08:00 UT on March 7–9 using ionospheric CIT. The space environment throughout this period was consistent. Observations recorded by 20 GNSS stations near the epicenter were used to invert the electron

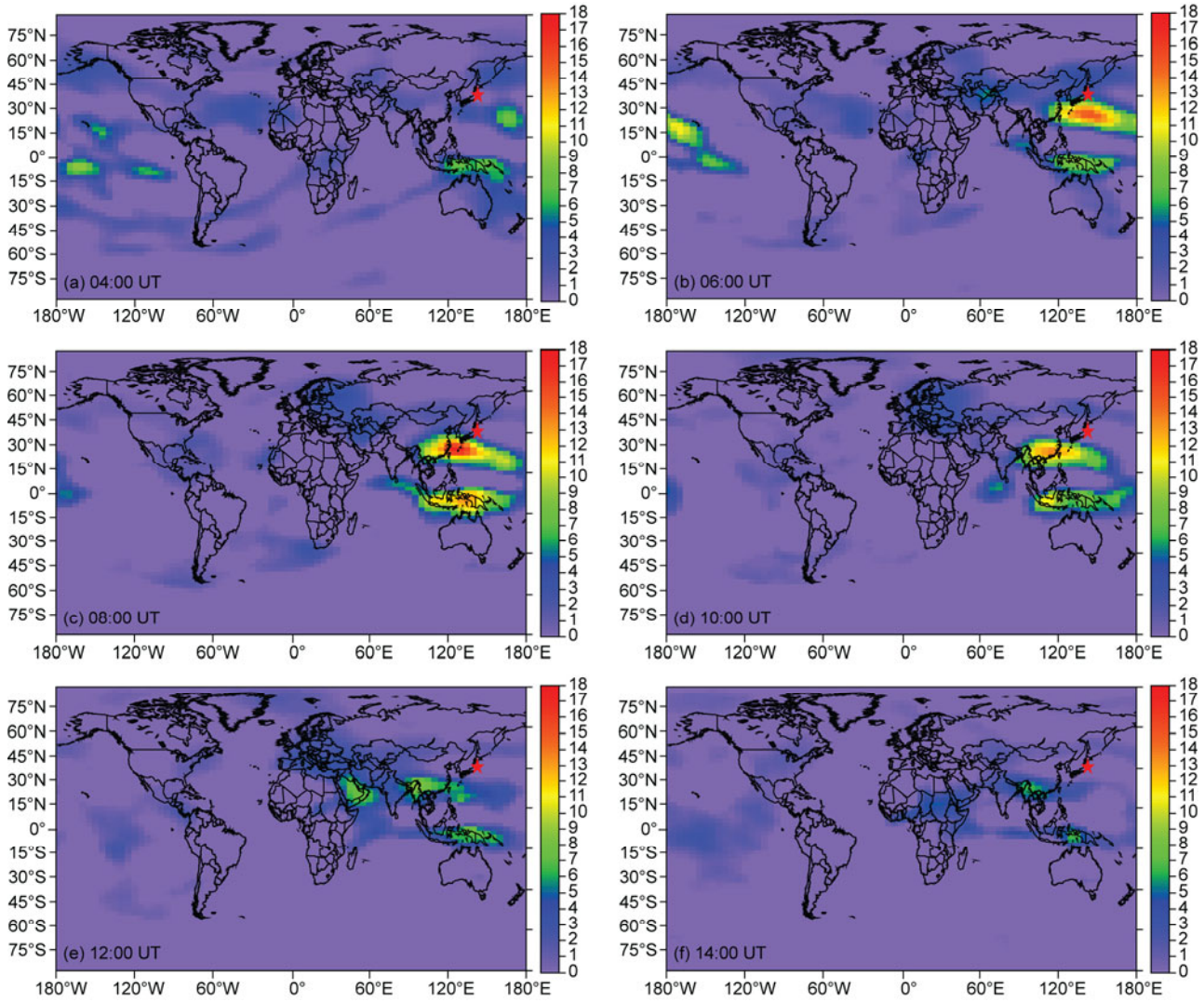

Figure 8 Global ΔVTEC maps from 04:00–14:00 UT on March 8 (unit: TECu), at time intervals of 2 h.

density. The inversion region is between 16°–40°N, 120°–140°E, and altitudes 100–1000 km. The grid size is 4°, 2° and 50 km in latitude, longitude and altitude, respectively. To obtain sufficient rays passing through the inversion region, we set the inversion period as 07:30–08:30 UT.

Figures 9, 10, and 11 show electron density distribution images at 126°, 130° and 134°E, respectively, during March 7–9. The unit is 10^{11} el/m^3.

Figures 9–11 show that the ionospheric electron density distributions for the three longitude slices are consistent on March 7 and 9, but on March 8 there was an overall increase in magnitude compared with those in the other two days. Changes in the ionospheric electron density along latitude lines were more significant than changes along meridians. From altitudes of 200 to 400 km, the ionospheric electron density changed more significantly than in other layers. Reviewing latitudinal changes in ionospheric electron density during these days, we found that positive anomalies between 18°–35°N were particularly evident, while changes in other latitude belts were small. The CIT analysis is consistent with the 2-D VTEC analysis, supporting our results.

3 Conclusion

We used VTEC data of four GNSS stations and f_oF_2 data of an ionosonde station near the epicenter to analyze ionospheric anomalies during the period surrounding the March 11, 2011 Japan earthquake. After analyzing the spatial distribution of the anomalies, we believe that the positive anomalies on March 8 are a likely seismo-ionospheric precursor of the earthquake.

Severe ionospheric anomalies on March 8 lasted from 04:00 to 14:00 UT, during which they gradually formed, increased and disappeared. The affected area of the ionosphere

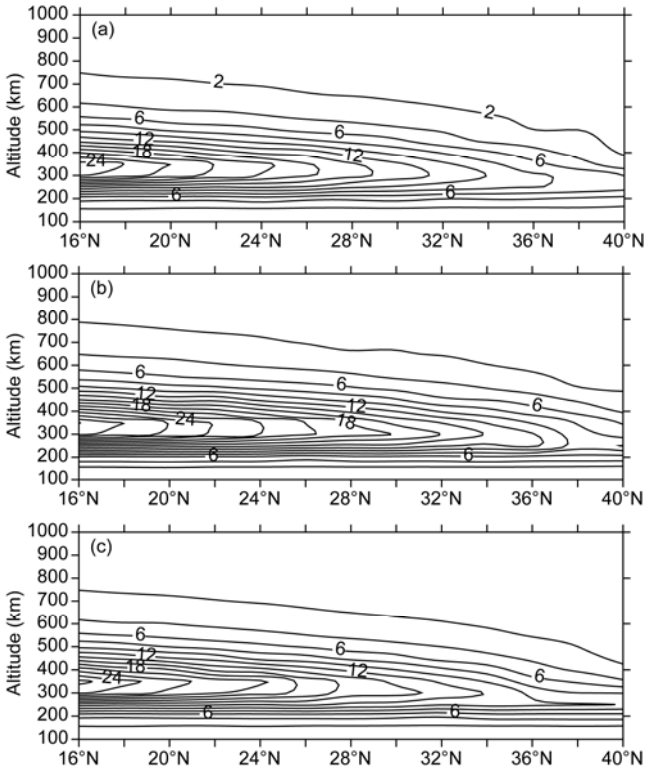

Figure 9 Electron density distribution images at 08:00 UT for March 7 (a), 8 (b) and 9 (c) at 126°E.

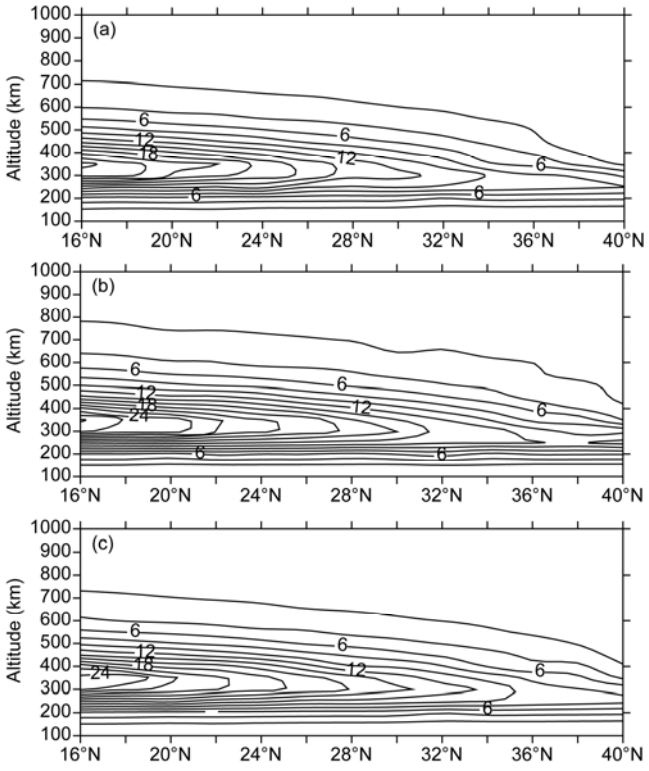

Figure 10 Electron density distribution images at 08:00 UT for March 7 (a), 8 (b) and 9 (c) at 130°E.

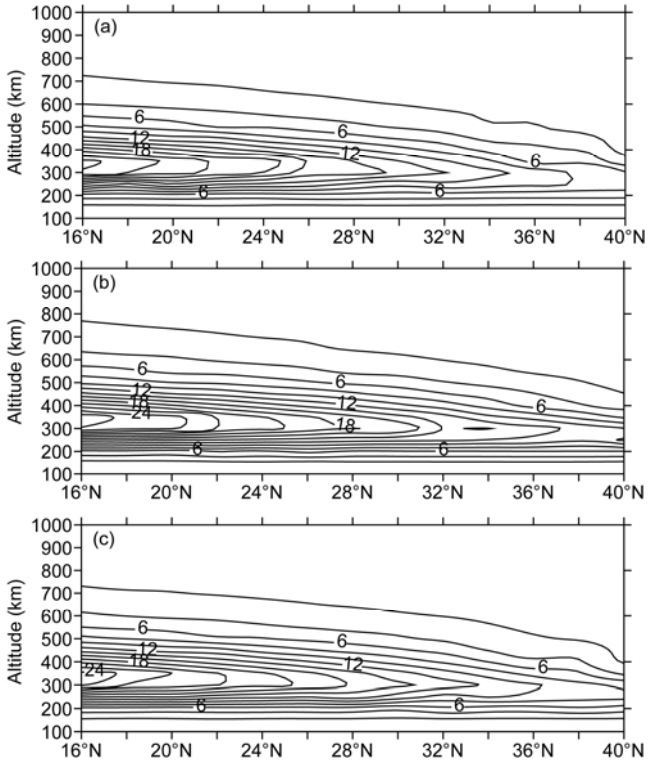

Figure 11 Electron density distribution images at 08:00 UT for March 7 (a), 8 (b) and 9 (c) at 134°E.

extended to longitude 50° and latitude 20°, with length ratio approximately 3∶1. The anomaly peak occurred between 08:00–10:00 UT; its location was not coincident with the vertical projection of the epicenter, but was to its south (equatorward). The maximum anomaly was 18 TECu greater than the associated upper bound. Corresponding ionospheric effects were also observed in the magnetically conjugated region. There was no contemporaneous, significant ionospheric VTEC anomaly in the rest of the world.

To aid understanding of changes in ionospheric electron density on March 8, we also used GNSS-based CIT technology to reconstruct the 3-D distribution of ionospheric electron density near the epicenter. The CIT result confirms that there were ionospheric anomalies on March 8. The ionospheric electron density on this day rose in comparison to the day before and after, and positive anomalies between 18°–35°N were especially apparent.

The results indicate that ionospheric anomalies occurring 0–5 days before an earthquake are likely to be seismic precursors. It is practical to study these anomalies for short-term earthquake prediction. However, the onset of earthquakes involves very complex processes, and it may be affected by many factors. There has not yet been a consensus about the physical mechanisms of pre-earthquake ionospheric anomalies. We can only provide a qualitative description of these anomalies. At present, we cannot accurately distinguish anomalies generated by solar or geomagnetic field

activity from those associated with earthquakes. Accurate earthquake prediction is a complex task that must consider various factors, and much research remains to be done.

The authors thank the IGS for providing GNSS observations and global ionosphere map data, the NASA and IUGG for providing solar and geomagnetic field data, and the NICT for providing ionosonde data. This work was accomplished at the Key Laboratory of Geospace Environment and Geodesy (Wuhan University), Ministry of Education, and it was supported by the Foundation for Innovative Research Groups of the National Natural Science Foundation of China (40721001) and the Surveying and Mapping Foundation Research Fund Program, State Bureau of Surveying and Mapping (10-02-13).

1 Zhu F Y, Wu Y, Lin J, et al. Anomalous response of ionospheric VTEC before the Wenchuan earthquake (in Chinese). Acta Seismol Sin, 2009, 31: 18022187
2 Yu T, Mao T, Wang Y G, et al. Study of the ionospheric anomaly before the Wenchuan earthquake (in Chinese). Chin Sci Bull (Chin Ver), 2009, 54: 1086–1092
3 Cai J T, Chen X B, Zhao G Z, et al. Earthquake precursor: the anomalies in the ionospheric F2 region (in Chinese). Prog Geophys, 2007, 22: 720–728
4 Li H H, Liu D F, Song X T. Some abnormal phenomena of the ionosphere peior to some great earthquake in China (in Chinese). Northwest Seismol J, 1984, 6: 1–11
5 Li Y S, Li K C. Ionospheric disturbances during large earthquakes (in Chinese). Acta Seismol Sin, 1987, 9: 101–107
6 Leonard R S, Barnes R A. Observation of ionospheric disturbances following the Alaska earthquake. J Geophys Res, 1965, 70: 1250–1253
7 Pulinets S A, Legen'ka A D, Gaivoronskaya T V, et al. Main phenomenological features of ionospheric precursors of strong earthquakes (in Chinese). J Atmos Sol Terr Phys, 2003, 65: 1337–1347
8 Fang H X, Weng L B, Wang W, et al. The use of the ionosphere in short–term earthquakes prediction (in Chinese). Sci Tech Eng, 2010, 10: 6698–6706
9 Liu J Y, Tsai H F, Lin C H, et al. Coseismic ionospheric disturbances triggered by the Chi-Chi earthquake. J Geophys Res, 2010, 115, A08303
10 Liu J Y, Chen Y I, Chuo Y J, et al. Variations of ionospheric total electron content during the Chi-Chi earthquake. Geophys Res Lett, 2001, 28: 1383–1386
11 Liu J Y, Chen Y I, Chuo Y J, et al. A statistical investigation of pre-earthquake ionospheric anomaly. J Geophys Res, 2006, 111: A05304
12 Dautermann T, Calais E, Haase J, et al. Investigation of ionospheric electron content variations before earthquakes in southern California, 2003–2004. J Geophys Res, 2006, 112: B02106
13 Weaver P F, Yuen P C, Prolss G W, et al. Acoustic coupling in the ionosphere from seismic waves of the earthquake at Kurile Islands on August 11. Nature, 1969, 226: 1239–1241
14 Antsilevich M G. The influence of Tashkent earthquake on the Earth's magnetic field and the ionosphere, Tashkent earthquake 26 April 1966. Tashkent FAN, 1971, 187–188
15 Pulinets S A, Boyarchuk K. Ionospheric Precursors of Earthquakes. Berlin: Springer, 2004
16 Pulinets S A. Seismic activity as a source of the ionospheric variability. Adv Space Res, 1998, 22: 903–906
17 Pulinets S A. Natural radioactivity, earthquakes, and the ionosphere. Eos Trans AGU, 2007, 88: 217–224
18 Liu J Y, Chen Y I, Pulinets S A, et al. Seismo-ionospheric signatures prior to $M\geqslant 6.0$ Taiwan earthquakes. Geophys Res Lett, 2000, 27: 3113–3116
19 Ding J H, Suo Y C, Su Y R. Phenomena of geomagnetic and ionospheric anomalies and their relation to earthquakes (in Chinese). Chin J Space Sci, 2005, 25: 536–542
20 Le H, Liu J Y, Liu L. A statistical analysis of ionospheric anomalies before 736 *M*6.0+ earthquakes during 2002–2010. J Geophys Res, 2011, 116: A02303
21 Calais E, Minster J B. GPS detection of ionospheric perturbations following the January 17, 1994 Northridge Earthquake. Geophys Res Lett, 1995, 22: 1045–1048
22 Zaslavski Y, Parrot M, Blanc E. Analysis of TEC measurements above active seismic regions. Phys Earth Planet Inter, 1998, 105: 219–228
23 Wu Y, Qiao X J, Zhou Y Y. Preseismic ionospheric TEC anomaly detected by ground-based GPS (in Chinese). J Geod Geodyn, 2005, 25: 36–40
24 Zhou Y Y, Wu Y, Qiao X J, et al. Anomalous variations of ionospheric VTEC before Ms 8.0 Wenchuan earthquake. Chin J Geophys, 2010, 53: 556–566
25 Liu J Y, Chen Y I, Chen C H, et al. Seismoionospheric GPS total electron content anomalies observed before the 12 May 2008 *M*w7.9 Wenchuan earthquake. J Geophys Res, 2009, 114: A04320
26 Zhao B, Wang M, Yu T, et al. Is an unusual large enhancement of ionospheric electron density linked with the 2008 great Wenchuan earthquake? J Geophys Res, 2008, 113: A11304
27 Lin J, Wu Y, Zhu F Y, et al. Wenchuan earthquake ionosphere TEC anomaly detected by GPS. Chin J Geophys, 2009, 52: 297–300
28 Zeng Z C, Zhang B, Fang G Y, et al. The analysis of ionospheric variations before Wenchuan earthquake with DEMETER data. Chin J Geophys, 2009, 52: 11–19
29 Ding Z H, Wu J, Su S J, et al. The variations of ionosphere on some days before the Wenchuan earthquake. Chin J Geophys, 2010, 53: 30–38
30 Zhu F Y, Wun Y, Lin J, et al. Study on ionospheric TEC anomaly prior to Wenchuan *M*s8.0 earthquake (in Chinese). J Geod Geodyn, 2008, 28: 16–21
31 Wu H. Investigation of GNSS-based ionospheric tomographic algorithms and their applications (in Chinese). Master's Dissertation. Wuhan: Wuhan University, 2011
32 Yang J, Wu Y, Zhou Y Y. Probe into seismo-ionospheric anomaly of Wenchuan *M*s8.0 earthquake based on computerized ionospheric tomography (in Chinese). J Geod Geodyn, 2011, 31: 9–14
33 Zou Y H. A study of time-dependent 3-D ionospheric tomography with ground-based GPS network and occultation observations (in Chinese). Dissertation for the Doctoral Degree. Wuhan: Wuhan University, 2004
34 Howe B M, Runciman K, Secan J A. Tomography of Ionosphere: Four-dimensional simulations. Radio Sci, 1998, 33: 109–128
35 Liu Z Z, Gao Y. Ionospheric tomography using GPS measurements. In: Proceedings of the International Symposium on Kinematic System in Geodesy, Geomatics and Navigation, Banff, Alberta, Canada, June 5–8. 2001. 111–120
36 Rius A, Ruffini G, Cucurull L. Improving the vertical resolution of ionospheric tomography with GPS occultations. Geophys Res Lett, 1997, 14: 2291–2294
37 Wen D B, Yuan Y B, Ou J K, et al. Ionospheric spatial and temporal variations during 18 August 2003 storm over China. Earth Planet Space, 2007, 59: 313–317
38 Thampi S V, Lin C, Liu H, et al. First tomographic observations of the Midlatitude Summer Nighttime Anomaly over Japan. J Geophys Res, 2009, 114: A10318
39 Li Z H, Huang J S. GPS Surveying and Data Processing (in Chinese). Wuhan: Wuhan University Press, 2005
40 Wen D B. Investigation of GPS-based ionospheric tomographic algorithms and their applications (in Chinese). Dissertation for the Doctoral Degree. Wuhan: Wuhan University, 2007
41 Liu S Z, Wang J X, Gao J Q. Inversion of ionospheric electron density based on a constrained simultaneous iteration reconstruction technique. IEEE Trans Geosci Remote Sens, 2010, 48: 2455–2459
42 Du P R, Jiang H R, Guo J S. Research on possibility of ionospheric anomalies as an earthquake precursor (in Chinese). Earthquake, 1998,

18: 19–126
43 Liu J Y, Chuo Y J, Shan S J, et al. Pre-earthquake ionospheric anomalies registered by continuous GPS TEC measurements. Ann Geophys, 2004, 22: 1585–1593
44 Oyama K I, Kakinami Y, Liu J Y, et al. Reduction of electron temperature in low latitude ionosphere at 600 km before and after large earthquakes. J Geophys Res, 2008, 113: A11317
45 Kim V P, Hegai V V. A Possible Presage of Strong Earthquakes in the Night-time Mid-latitude Region Ionosphere, Atmospheric and Ionospheric Electromagnetic Phenomena Associated with Earthquake. Tokyo: Terra Scientific Publishing Company, 1999. 619–627
46 Liu J Y, Le H, Chen Y I, et al. Observations and simulations of seismoionospheric GPS total electron content anomalies before the 12 January 2010 *M*7 Haiti earthquake. J Geophys Res, 2011, 116: A04302